Supplement of Atmos. Chem. Phys., 19, 7897–7911, 2019
https://doi.org/10.5194/acp-19-7897-2019-supplement

Atmospheric Chemistry and Physics
Open Access
EGU

Supplement of

Chemical characterization and sources of submicron aerosols in the northeastern Qinghai–Tibet Plateau: insights from high-resolution mass spectrometry

Xinghua Zhang et al.

Correspondence to: Jianzhong Xu (jzxu@lzb.ac.cn)

Figures

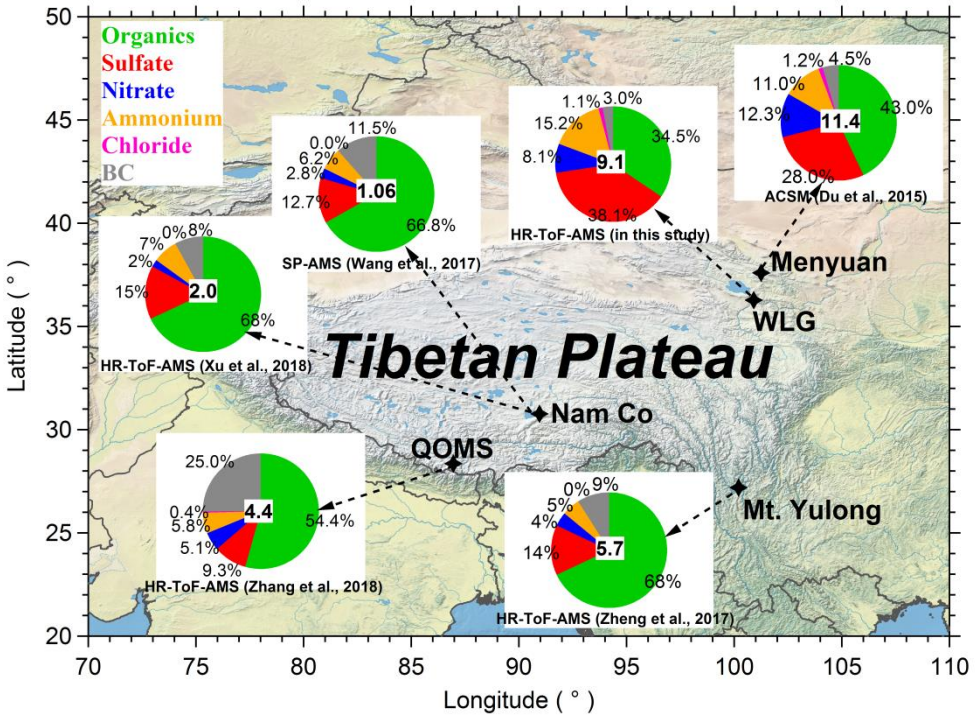

Figure S1. The field studies conducted at high elevation sites in the Qinghai-Tibet Plateau using AMS or ACSM measurements. The mass concentrations of PM_1 and the mass contributions of each chemical species (pie chart) are presented in each site.

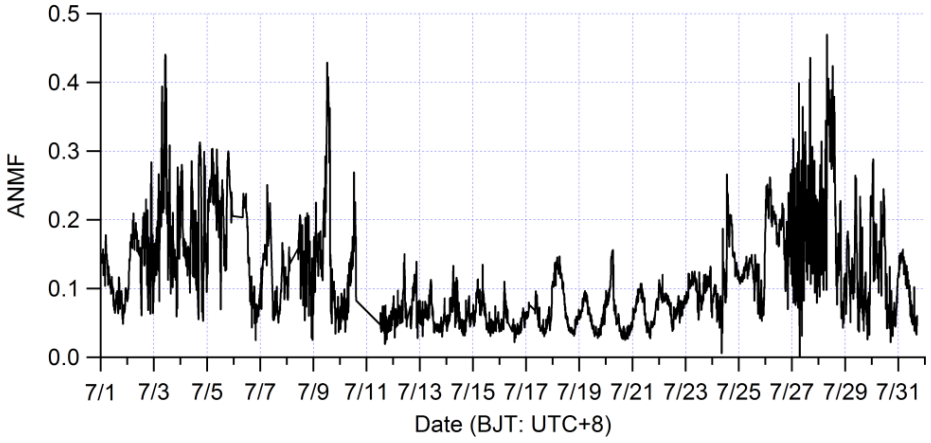

Figure S2. The time series of ANMF (ANMF = $(80/62\times NO_3)/(NH_4 + SO_4 + NO_3 + Chl + Org)$) in this study.

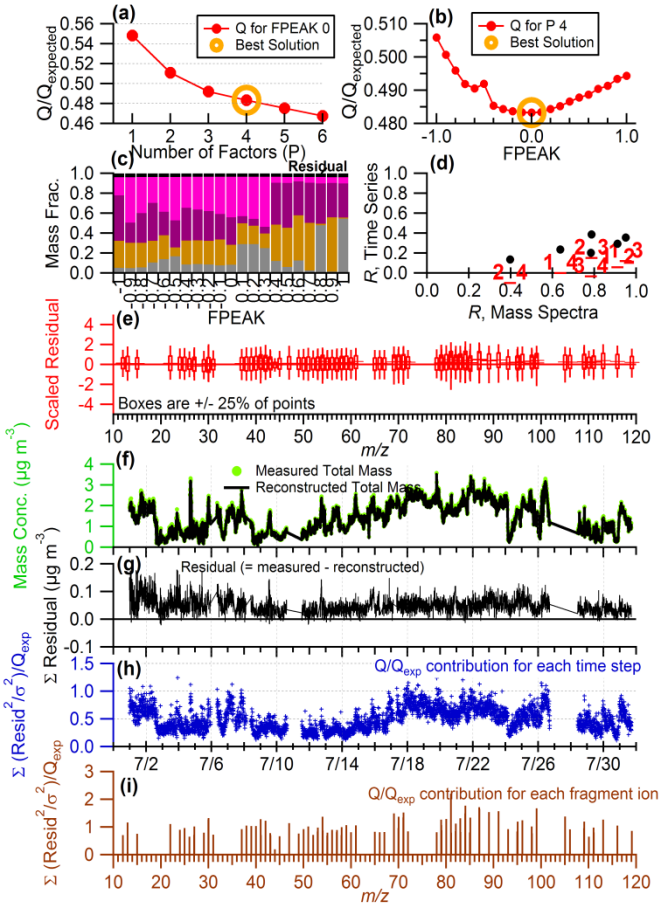

Figure S3. Summary of key diagnostic plots of the PMF results: **(a)** Q/Q_{exp} as a function of factor number (p) that selected for PMF analysis. For the best solution (four factors solution): **(b)** Q/Q_{exp} as a function of *f*Peak, **(c)** fractions of OA factors vs. *f*Peak, **(d)** correlations among PMF factors, **(e)** the box and whiskers plot showing the distributions of scaled residuals for each m/z, **(f)** time series of the measured organic mass and the reconstructed organic mass, **(g)** variations of the residual (= measured - reconstructed) of the fit, **(h)** the Q/Q_{exp} for each point in time, and **(i)** the Q/Q_{exp} values for each ion.

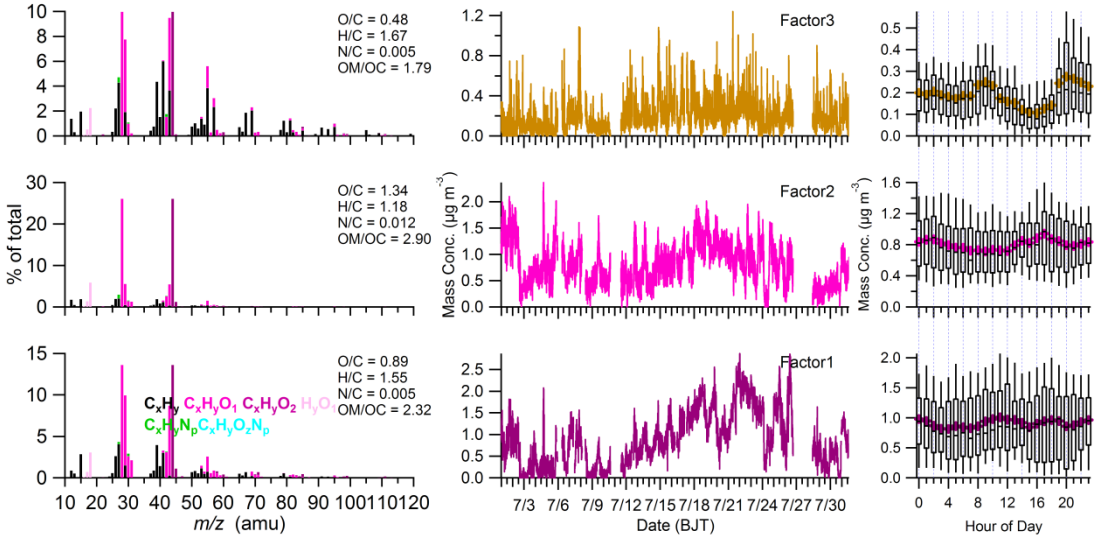

Figure S4. The 3-factor solution PMF results: **(left)** high-resolution mass spectrum of three OA factors colored by six ion categories at m/z < 120, **(middle)** time series of the three OA factors, and **(right)** diurnal variations of mass concentrations of the three OA factors (the whiskers above and below the boxes indicate the 90th and 10th percentiles, the upper and lower boundaries respectively indicate the 75th and 25th percentiles, the lines in the boxes indicate the median values, and the cross symbols indicate the mean values).

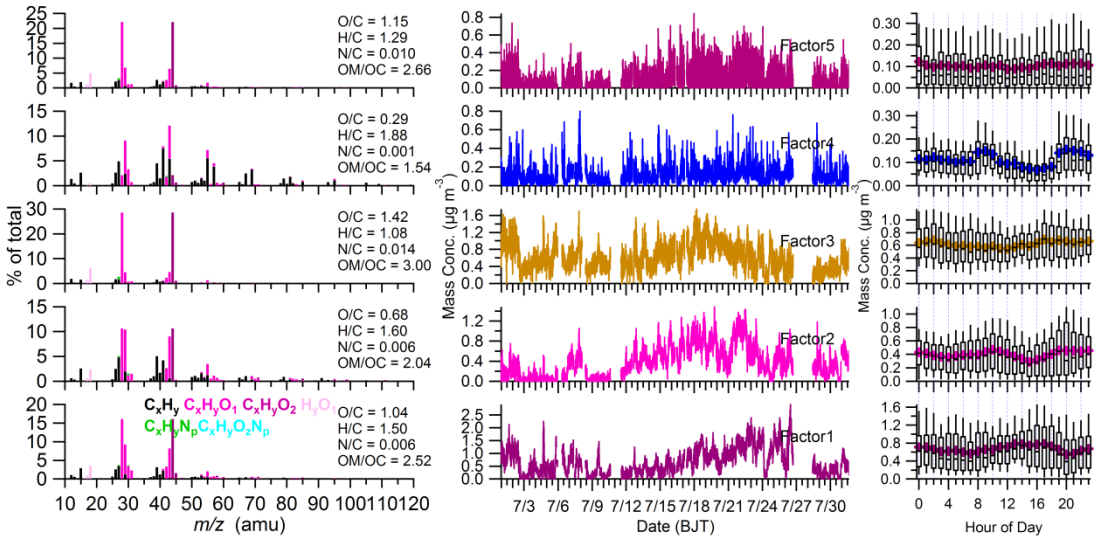

20 **Figure S5.** The 5-factor solution PMF results: **(left)** high-resolution mass spectrum of five OA factors colored by six ion categories at m/z < 120, **(middle)** time series of the five OA factors, and **(right)** diurnal variations of mass concentrations of the five OA factors (the whiskers above and below the boxes indicate the 90th and 10th percentiles, the upper and lower boundaries respectively indicate the 75th and 25th percentiles, the lines in the boxes indicate the median values, and the cross symbols indicate the mean values).

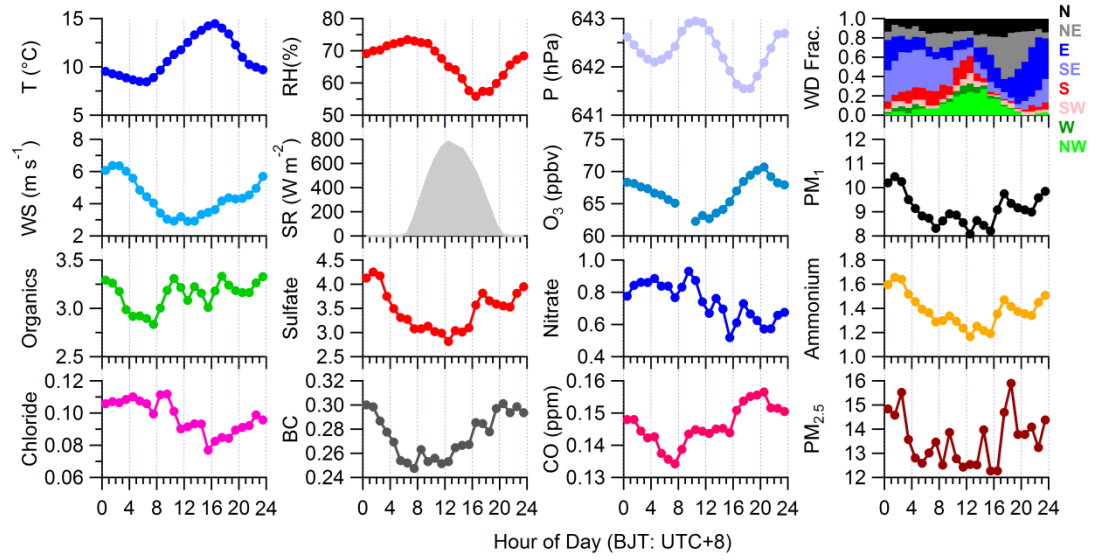

25 **Figure S6.** Diurnal variations of meteorological conditions, PM_1 chemical species and other relevant gaseous and particulate parameters.

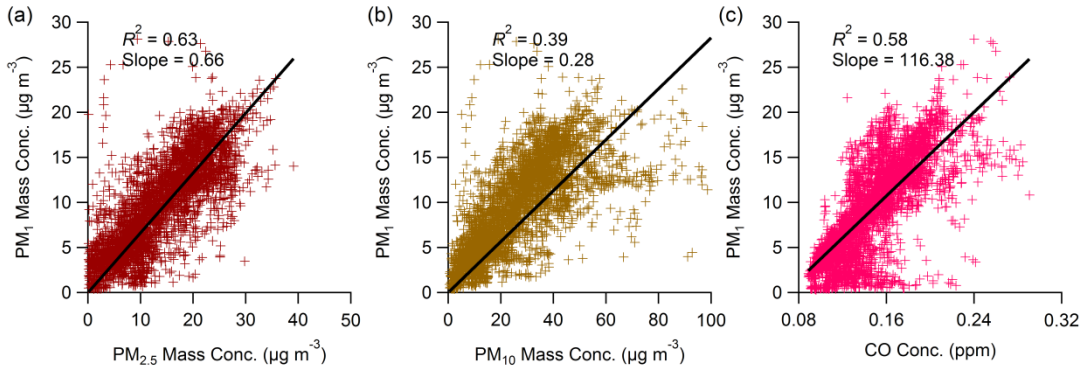

Figure S7. Scatterplots of mass concentrations of **(a)** PM_1 vs. $PM_{2.5}$, **(b)** PM_1 vs. PM_{10}, and **(c)** PM_1 vs. CO in this study.

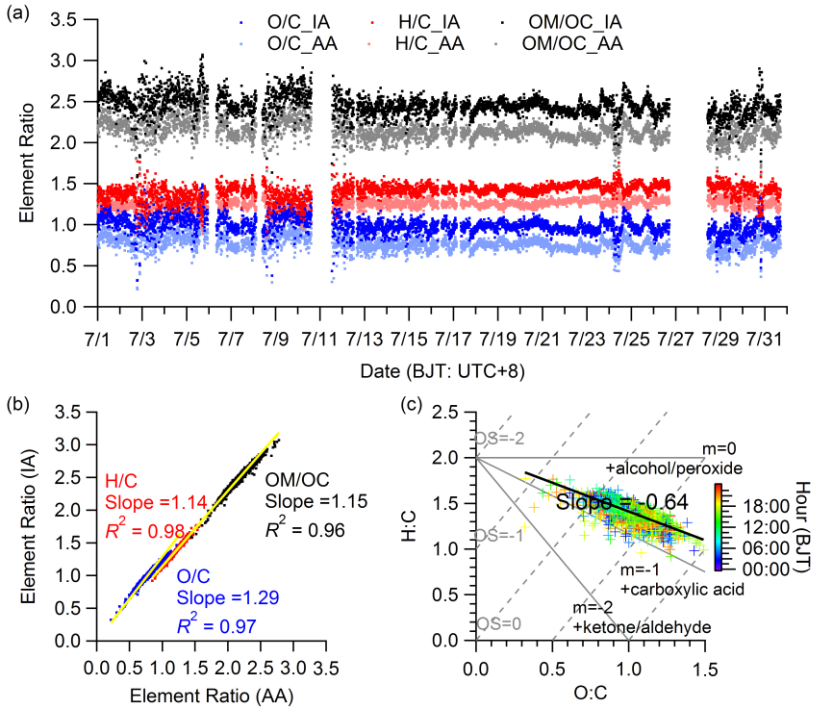

Figure S8. (a) Comparison of the temporal variations of O/C, H/C, and OM/OC ratios using "Improved-ambient" method versus "Aiken ambient" method for the whole study period, **(b)** scatterplot of elemental ratios with "Improved-ambient" method versus that with "Aiken ambient" method and **(c)** Van Krevelen diagram of H/C versus O/C for OA in this study.

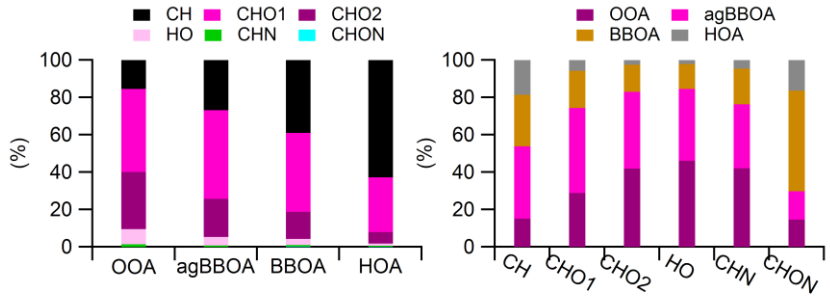

Figure S9. The contributions of **(left)** six ionic categories to PMF factors and **(right)** PMF factors to six ionic categories.

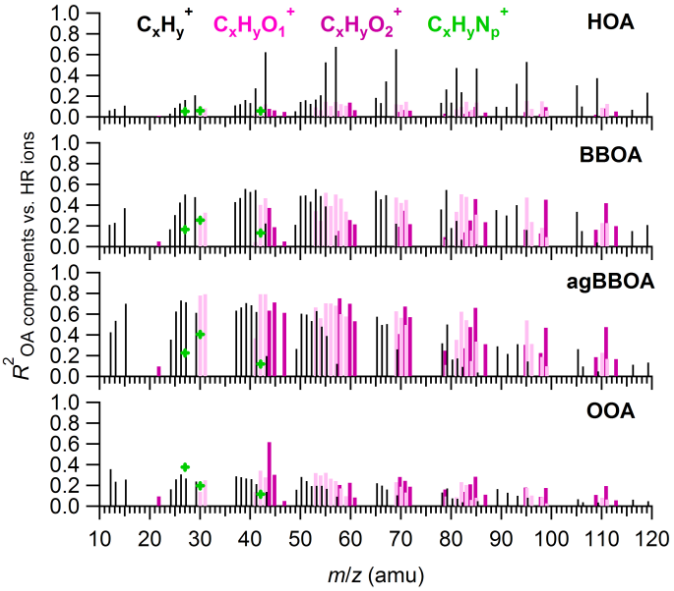

Figure S10. Correlations between each organic component and HRMS ions colored by four ion categories ($C_xH_y^+$, $C_xH_yO^+$, $C_xH_yO_2^+$, $C_xH_yN_p^+$).

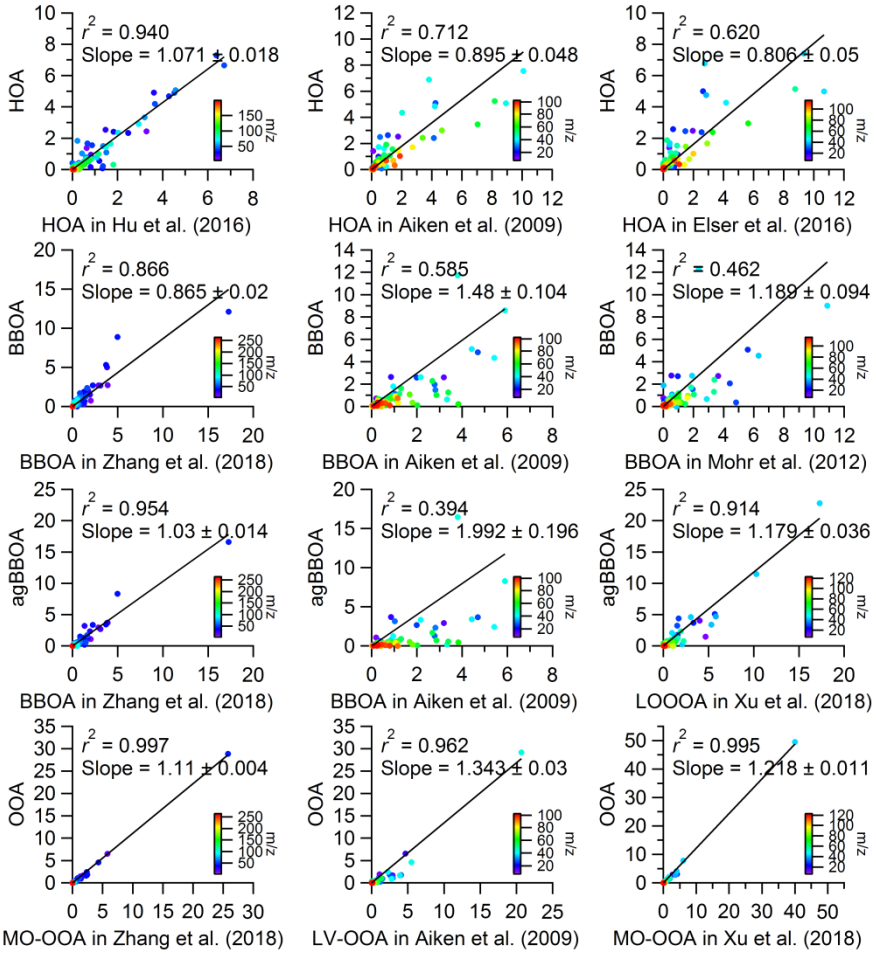

Figure S11. Scatter plots of the comparisons between the four high-resolution mass spectra identified in this study and those high-resolution mass spectra determined from other studies.

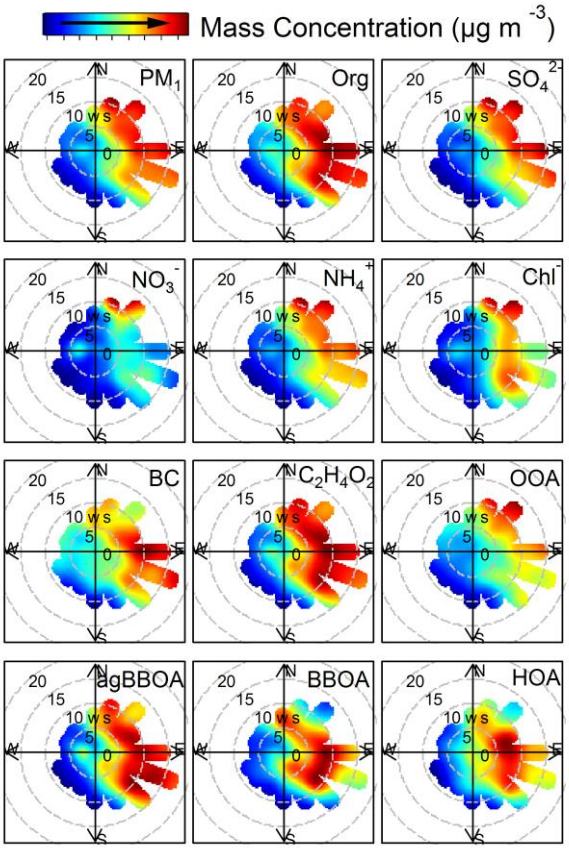

Figure S12. Bivariate polar plots that illustrate the variations of mass concentrations (colored) of each PM_1 species and organic components as a function of wind speed (m s^{-1}) and wind direction in this study.

References

Aiken, A. C., Salcedo, D., Cubison, M. J., Huffman, J. A., DeCarlo, P. F., Ulbrich, I. M., Docherty, K. S., Sueper, D., Kimmel, J. R., Worsnop, D. R., Trimborn, A., Northway, M., Stone, E. A., Schauer, J. J., Volkamer, R. M., Fortner, E., de Foy, B., Wang, J., Laskin, A., Shutthanandan, V., Zheng, J., Zhang, R., Gaffney, J., Marley, N. A., Paredes-Miranda, G., Arnott, W. P., Molina, L. T., Sosa, G., and Jimenez, J. L.: Mexico City aerosol analysis during MILAGRO using high resolution aerosol mass spectrometry at the urban supersite (T0)–Part 1: Fine particle composition and organic source apportionment, Atmos. Chem. Phys., 9, 6633-6653, doi:10.5194/acp-9-6633-2009, 2009.

Du, W., Sun, Y. L., Xu, Y. S., Jiang, Q., Wang, Q. Q., Yang, W., Wang, F., Bai, Z. P., Zhao, X. D., and Yang, Y. C.: Chemical characterization of submicron aerosol and particle growth events at a national background site (3295 m a.s.l.) on the Tibetan Plateau, Atmos. Chem. Phys., 15, 10811-10824, doi:10.5194/acp-15-10811-2015, 2015.

Elser, M., Huang, R.-J., Wolf, R., Slowik, J. G., Wang, Q., Canonaco, F., Li, G., Bozzetti, C., Daellenbach, K. R., Huang, Y., Zhang, R., Li, Z., Cao, J., Baltensperger, U., El-Haddad, I., and Prévôt, A. S. H.: New insights into PM_{2.5} chemical composition and sources in two major cities in China during extreme haze events using aerosol mass spectrometry, Atmos. Chem. Phys., 16, 3207-3225, doi:10.5194/acp-16-3207-2016, 2016.

Hu, W. W., Hu, M., Hu, W., Jimenez, J. L., Yuan, B., Chen, W., Wang, M., Wu, Y., Chen, C., Wang, Z., Peng, J., Zeng, L., and Shao, M.: Chemical composition, sources, and aging process of submicron aerosols in Beijing: Contrast between summer and winter, J. Geophys. Res. Atmos., 121, 1955-1977, doi:10.1002/2015jd024020, 2016.

Mohr, C., DeCarlo, P. F., Heringa, M. F., Chirico, R., Slowik, J. G., Richter, R., Reche, C., Alastuey, A., Querol, X., Seco, R., Peñuelas, J., Jiménez, J. L., Crippa, M., Zimmermann, R., Baltensperger, U., and Prévôt, A. S. H.: Identification and quantification of organic aerosol from cooking and other sources in Barcelona using aerosol mass spectrometer data, Atmos. Chem. Phys., 12, 1649-1665, doi:10.5194/acp-12-1649-2012, 2012.

Wang, J., Zhang, Q., Chen, M., Collier, S., Zhou, S., Ge, X., Xu, J., Shi, J., Xie, C., Hu, J., Ge, S., Sun, Y., and Coe, H.: First Chemical Characterization of Refractory Black Carbon Aerosols and Associated Coatings over the Tibetan Plateau (4730 m a.s.l), Environ. Sci. Technol., 51, 14072-14082, doi:10.1021/acs.est.7b03973, 2017.

Xu, J., Zhang, Q., Shi, J., Ge, X., Xie, C., Wang, J., Kang, S., Zhang, R., and Wang, Y.: Chemical characteristics of submicron particles at the central Tibetan Plateau: insights from aerosol mass spectrometry, Atmos. Chem. Phys., 18, 427-443, doi:10.5194/acp-18-427-2018, 2018.

Zhang, X., Xu, J., Kang, S., Liu, Y., and Zhang, Q.: Chemical characterization of long-range transport biomass burning emissions to the Himalayas: insights from high-resolution aerosol mass spectrometry, Atmos. Chem. Phys., 18, 4617-4638, doi:10.5194/acp-18-4617-2018, 2018.

Zheng, J., Hu, M., Du, Z., Shang, D., Gong, Z., Qin, Y., Fang, J., Gu, F., Li, M., Peng, J., Li, J., Zhang, Y., Huang, X., He, L., Wu, Y., and Guo, S.: Influence of biomass burning from South Asia at a high-altitude mountain receptor site in China, Atmos. Chem. Phys., 17, 6853-6864, doi:10.5194/acp-17-6853-2017, 2017.